International Forum on Aeroelasticity and Structural Dynamics
IFASD 2019
9-13 June 2019, Savannah, Georgia, USA

DESIGN AND VALIDATION OF A NUMERICAL HIGH ASPECT RATIO AEROELASTIC WIND TUNNEL MODEL (HMAE1)

H.S. Timmermans[1], J.H. van Tongeren[1], E.G.M Geurts[1]
R.F.A. Marques[2], M.S. Correa[2]
S. Waitz[3]

[1] Netherlands Aerospace Centre (NLR)
Anthony Fokkerweg 2, 1059CM Amsterdam, the Netherlands
huub.timmermans@nlr.nl

[2] Embraer S.A.
São José dos Campos, Brazil
rodrigo.marques@embraer.com.br

[3]German Aerospace Center (DLR), Institute of Aeroelasticity
Bunsenstr. 10, 37073 Göttingen, Germany
stefan.waitz@dlr.de

Keywords: aeroelasticity, structural dynamics, windtunnel testing, finite element modeling

Abstract: The aircraft manufacturer Embraer, the German Aerospace Center (DLR), the Netherlands Aerospace Centre (NLR) and German–Dutch Wind Tunnels (DNW) have tested an innovative highly flexible wing within an aeroelastic wind tunnel experiment in the transonic regime. The HMAE1 project was initiated by Embraer to test its numerical predictions for wing flutter under excessive wing deformations in the transonic regime. A highly elastic fiberglass wing-body pylon nacelle wind tunnel model, which is able to deform extensively, was constructed for the experiment. The model was instrumented with a large number of pressure orifices, strain gauges, stereo pattern recognition markers and accelerometers. The wing was tested from M = 0.4 till M = 0.9 for different angles of attack and stagnation pressure. The HMAE1 model was tested in two different test campaigns in which the Mach number was increased. This paper will focus on the first test campaign of the HMAE1 project in which the windtunnel model is tested up to M = 0.7 and will describe the development of the physical numerical structural dynamic MSC Nastran model representing the manufactured windtunnel model in order to perform numerical aeroelastic analyses.

Abbreviations:

AoA = Angle of Attack
ASE = Aero-ServoElastic
BC = Boundary Conditions
DLR = German Aerospace Center
DNW = German–Dutch Wind Tunnels
DNW-HST = DNW transonic windtunnel
FEM = Finite Element Model
FRF = Frequency Response Function
GVT = Ground Vibration Test
HMAE1 = Half Model AeroElastic (project acronym)
LAD = Load Application Devices
LE = Leading Edge
M = Mach number
MAC = Modal Assurance Criterion
NLR = Netherlands Aerospace Centre
PSD = Power Spectral Density
RMS = Root Mean Square
SPR = Stereo Pattern Recognition
TE = Trailing Edge

1 INTRODUCTION

The Brazilian aircraft manufacturer Embraer, the German Aerospace Center (DLR), the Netherlands Aerospace Centre (NLR) and German–Dutch Wind Tunnels (DNW) have succeeded in testing an innovative method for examining the safety of future aircraft. In another first, they have been able to analyze the flutter behavior of a wing in real time [1][2].
The HMAE1 (Half Model AeroElastic) project was initiated by Embraer to test its numerical predictions for wing flutter under excessive wing deformations in the transonic regime. The main objectives set for the project can be summarized as follows:

- an aeroelastic wing model with high deflection;
- a target for the first five prescribed modeshapes and frequencies;
- a target for the required flutter mechanism;
- a target for the dynamic aeroelastic model behavior in terms of damping.

In order to fulfill the objectives, a highly elastic fiberglass wing-body pylon nacelle wind tunnel model (see Figure 1), which is able to deform extensively, was constructed for the experiment. The model was instrumented with a large number of pressure orifices, strain gauges, Stereo Pattern Recognition (SPR) markers and accelerometers. The wing was tested from M = 0.4 to M = 0.9 for different angles of attack and stagnation pressure. The static and dynamic behavior of the wing model was monitored and a new method to analyze its Eigen frequencies and damping ratios was used, [3][4].

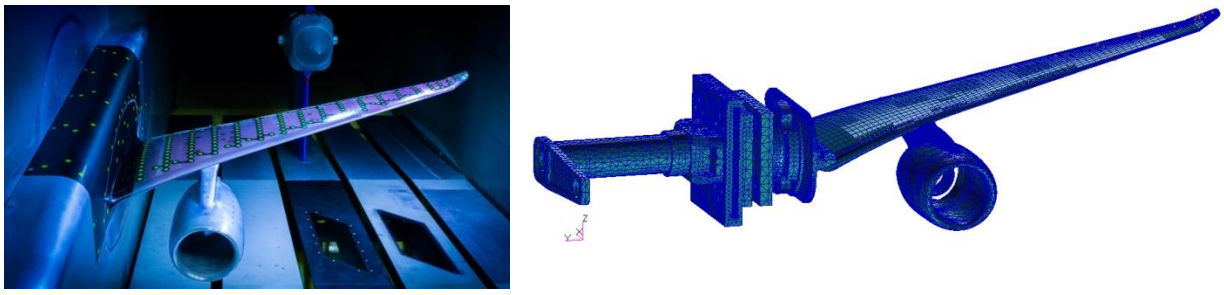

Figure 1: (left) HMAE1 aeroelastic windtunnel model (including the SPR markers on the top side) inside the DNW-HST windtunnel, (right) numerical MSC Nastran Finite Element Model including detailed boundary conditions

In order for Embraer to increase the quality of their tools and predictions, a high fidelity and validated numerical model is required that represents the static and dynamic characteristics of the manufactured wind tunnel model. Within the HMAE1 project, a numerical Finite Element Model (FEM) has been generated within the MSC Nastran format to represent the manufactured HMAE1 wind tunnel model, see Figure 1. This model is extensively correlated with the more detailed Abaqus FEM and, after the manufactured model was available, with Ground Vibration Tests (GVT's). The model has been updated and adjusted to provide a high correlated match between the actual manufactured model and the FEM. During the design phases of the HMAE1 project, the numerical MSC Nastran model has been used to assess critical loading cases based on the windtunnel test matrix as input to the Abaqus stress FEM. In addition to the loads analyses, a large amount of flutter analyses has been done in order to match requirements set by Embraer which was to clearly show the beginning of deterioration of damping for the flutter mechanism inside the test matrix.

The paper will describe the numerical MSC Nastran model, load and flutter analyses performed during the design and the correlation of the numerical model with test result data.

2 DESIGN OF THE NUMERICAL FINITE ELEMENT MODEL

Within the HMAE1 project, two finite element models are created and used to evaluate the model in terms of strength (Abaqus model) and the intended static and dynamic aeroelastic properties (MSC Nastran model). The preliminary design resulted in a converged concept design and was described, discussed and finalized in a preliminary design review. Based on this first concept design, an Abaqus FEM was created in order to evaluate strength using a first (rigid) loads estimation and to include manufacturing aspects. Based on the CAD model and Abaqus FEM a physical (structural dynamic) MSC Nastran FEM is created which is later on updated to match the wind tunnel model based on GVT's. This chapter describes the generation of the MSC Nastran model.

2.1 Wing

The wing consists of different components; the upper and lower skins, a foam core, the D-spar, instrumentation pockets and corresponding instrumentation masses. The wing consists of glass fiber reinforced plastic skins which are modelled using PCOMP elements in combination with MAT8 cards to specify the composite properties. To avoid duplication of mass at the Trailing Edge (TE) the PCOMP elements are generated in a way that the thickness is varied chord wise. The last elements at the TE of the wing skin are connected via a shared node between the solid foam material and wing skin node. The wing skin is modelled using element offsets in such a way that the shell elements represent the outside of the skin. The D-spar was added to the model for extra structural strength and is positioned in the Leading Edge (LE) of the wing. The inner core, represented by foam material, was modelled using HEX8 solid elements. Concentrated mass points are included in the model representing the accelerometer mass locations, remainder instrumentation mass and an inertia correction at each sectional center of gravity to match the inertia properties of the Abaqus FEM.

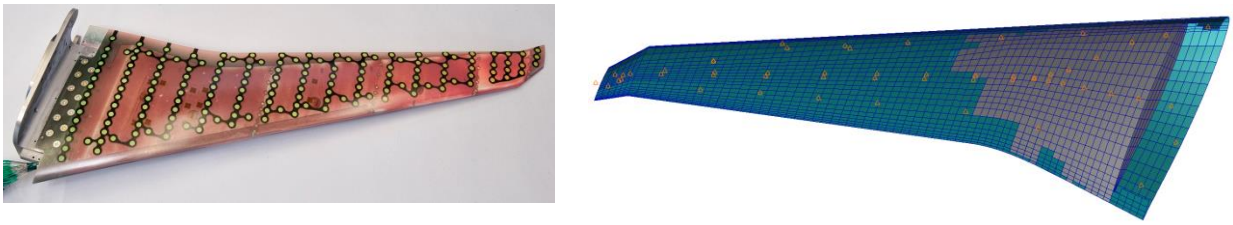

Figure 2: (left) manufactured wing skin (upper part), (right) FEM model including wing skin, foam and concentrated masses for instrumentation

The wingtip is a separated part which was bonded between the wing skins and contains the accelerometers of the wing tip region and pockets for application of additional masses to vary the mass distribution within a determined range. These masses allow tuning the dynamic behavior of the model after manufacturing before entering the wind tunnel.

2.2 Pylon-nacelle

The pylon consists of two main parts: the upper pylon and the lower pylon. The upper pylon is connected to the lower pylon and nacelle by means of local RBE2 connections at the bolt locations (pink locations), see Figure 3. The inner core is a separate part connected by means of a large RBE2 covering the intake area where the inner core is attached to the lower pylon.

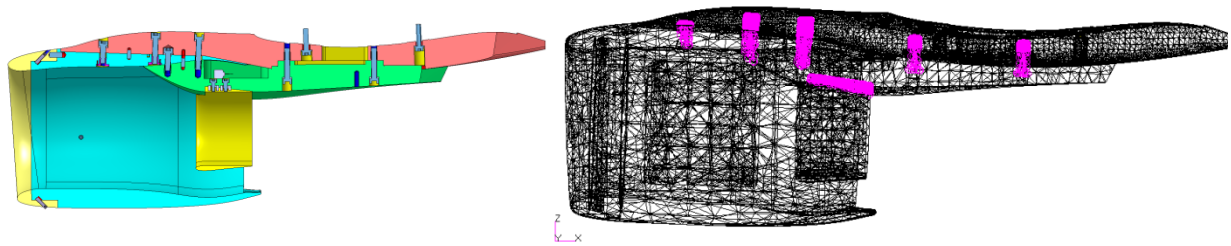

Figure 3: (left) CATIA model of the pylon (upper and lower) and nacelle, (right) FEM including the bolt connections between the components

The upper pylon is connected to the lower wing skin by means of a contact pad on the upper pylon and support pads inside the lower wing skin in order to distribute the loads into the skin. Within the FEM the connection is modelled by means of a rigid connection to represent the bolts and adjustable stiffness elements to represent the contact stiffness between the upper pylon and lower wing skin.

2.3 High fidelity boundary conditions

During the development of the structural dynamic FEM it was decided to include a high fidelity representation of the Boundary Condition (BC) (windtunnel interface parts). The boundary conditions have a significant effect upon the structural dynamic characteristics of the model and therefore on the aeroelastic flutter phenomena. Due to the fact the model was tested to have a clear and measurable deterioration of damping for the flutter mechanism inside the test matrix, the numerical FEM as input to the flutter analyses was required to be as accurate as possible to predict the flutter behavior.

The windtunnel-to-model interface consists of different components; the balance, the axle to balance adapter, the axle itself and a lever to allow for pitch control of the model, see Figure 4. Within the balance model, the piezo elements are included by means of variable stiffness elements.

The right side of Figure 4 shows the effect of the high fidelity boundary conditions upon the pylon pitch mode. A large effect in mode shape is evident while the difference in frequency was roughly 3%.

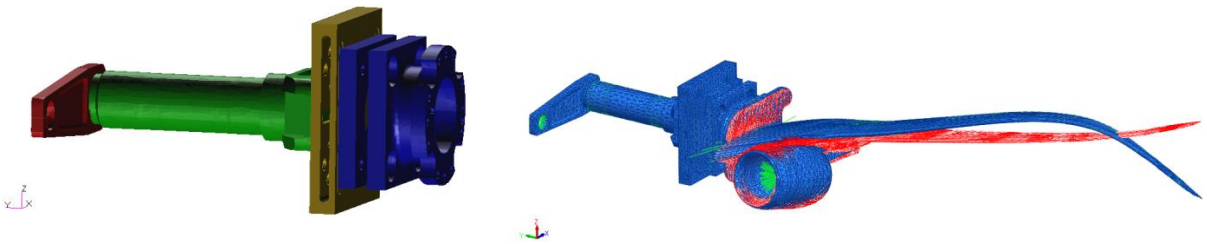

Figure 4: (left) High fidelity boundary FEM and (right) effect upon the pylon pitch mode with the blue model including the high fidelity BC.

3 LOADS AND FLUTTER ANALYSES

During the design phases, loads and flutter analyses have been performed using the numerical MSC Nastran model.

3.1 Static and dynamic loads analyses

Three different loading cases have been analyzed within the project, static load cases for different test points inside the test matrix, turbulence loads and loads due to a pitch excitation introduced at the lever. All of the load cases have been analyzed using MSC Nastran aeroelastic solvers including a camber correction for the airfoils.

3.1.1 Static loadcase

Based on an extensive loads analyses study during the preliminary design phase for different test conditions inside the test matrix, some static load cases were considered critical. The result was 19% maximum tip deflection of the semi span, see Figure 5, and a twist distribution as shown in Figure 6. The model is analyzed with a static aeroelastic loads analyses including elastic effects. The loads have been used as input for the Abaqus FEM to assess the strength of the model including the required safety factor set by DNW.

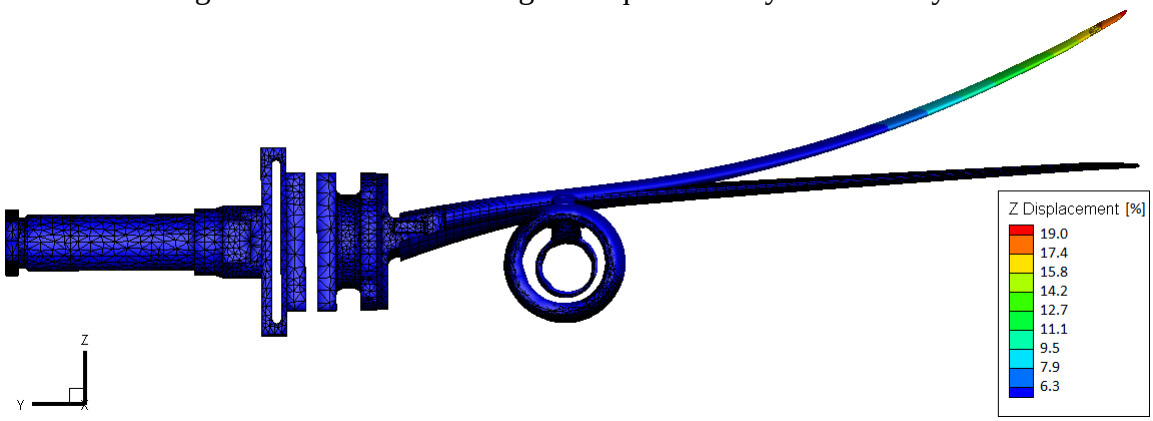

Figure 5: Deformation of the wing under the critical static aero load. Deformation scale factor = 1.0

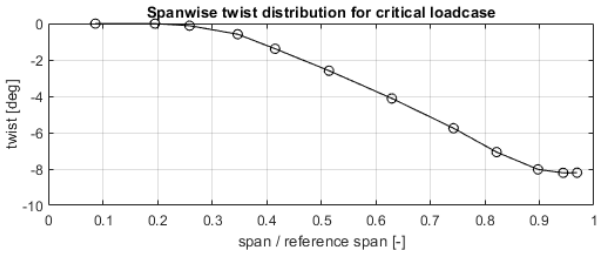

Figure 6: Spanwise twist distribution of the wing under the critical static aero load

3.1.2 Dynamic loads

Dynamic loads have been analyzed for both the turbulence conditions inside the windtunnel as well as a prescribed pitch excitation. The turbulence loads have been calculated based on the measured turbulence levels assuming a random gust analysis. The turbulence loads are calculated at the critical test condition. The condition input used for the gust spectra assumed a gust velocity equal to 1 over the velocity, which is equal to unit gust velocity amplitude. The scale length and amplitude of the gust were modeled by fitting a von Kármán spectrum to the Power Spectral Density (PSD) of the differential pressure measured inside the windtunnel, and corresponding pressure and airflow velocity through acoustics fundamentals. Figure 7 shows the response of the accelerometer locations which have been installed in the wing for the turbulence dynamic loadcase. The largest response was obtained from the tip accelerometers.

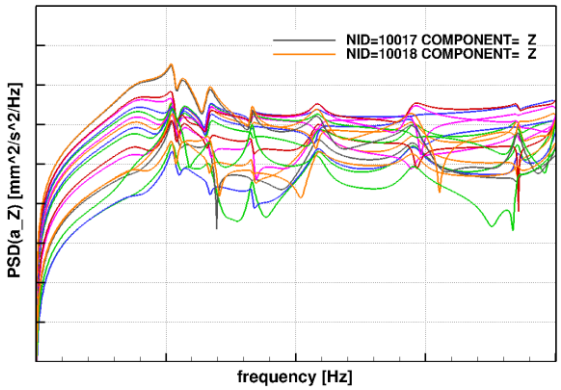

Figure 7: PSD acceleration response for the accelerometer locations installed in the windtunnel model

The results from the dynamic aeroelastic gust response analyses, in terms of a RMS force, at various spanwise locations, is provided as input to the Abaqus model in order to assess the strength of the model.

During the design phases, it was unknown whether the turbulence levels inside the wind tunnel would be sufficient to dynamically excite the model. Due to this uncertainty, it was decided to excite the model at every test point using a pulse pitch excitation introduced at the lever position. In order to reduce the dynamic loads, short pitch excitations of 0.1 [sec] and 0.5 [deg] were selected to excite the model, as shown in Figure 8 (left). The dynamic response is assessed at various spanwise locations, see Figure 8 (right) and the maximum loads have been provided as input to the Abaqus stress FEM.

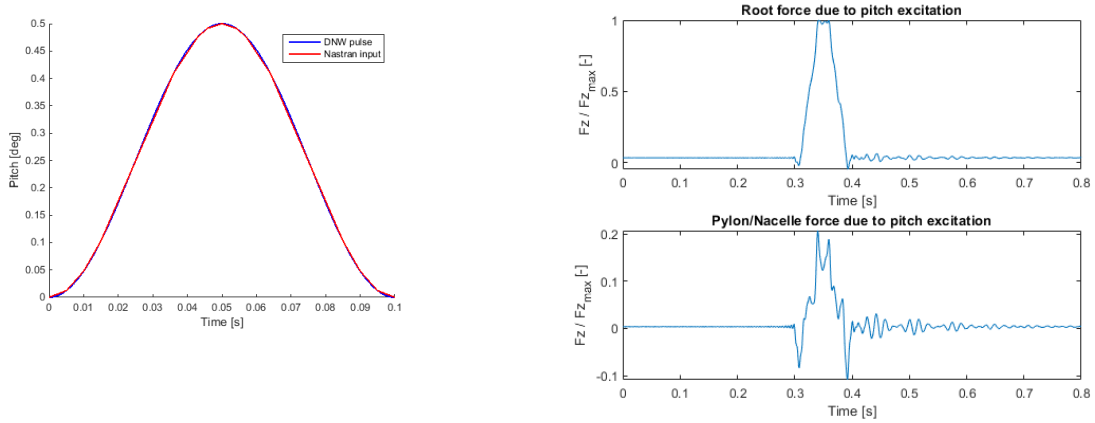

Figure 8: (left) pitch excitation pulse, defined by DNW and MSC Nastran input, (right) dynamic response of the model at the root and pylon-wing attachment

Both the turbulence and the pitch excitation load cases have been analyzed for various mass cases to see the effect of the tuning masses. The worst condition has been used to assess the model strength.

3.2 Flutter analyses

In accordance to the campaign test matrix, the aeroelastic stability behavior of the HMAE1 wing had been investigated in various flutter calculations, with a special interest in the pre-flutter stability decrease as set as target by Embraer. These damping design target areas, for both the maximum damping of the flutter mode and zero values (flutter points) have been marked red in the damping curves shown in Figure 11.

While making use of the MSC Nastran interface to incorporate the structural modal basis, the ZAERO aeroelastic code (version 9.0) served as flutter solver. Both matched Mach number and non-matched point analyses have been conducted, while activating the respective suitable flutter module in the open control loop calculations for the case of elastic BC (FLUTTER module) as well as in the closed control loop calculations for the aero-servoelastic cases (ASE module).

3.2.1 Model build-up of the aeroelastic system and the ASE control loops

The structural model of the wing with attached pylon and engine nacelle had been designed in a way which provided for a prescribed frequency distribution and order of the lower Eigen modes. The complete aeroelastic simulation model of the HMAE1 wing can be separated into the three main subgroups “wing structure”, “aerodynamic model” and “elastic BC”. These have been developed in an iterative process under the application of several design criteria (e.g. the maximum deflection), while the resulting dynamic aeroelastic behavior was studied in different combinations of BC and wing structure (e.g. with additional nacelle and wing tip masses). The eventual design of each of the three subgroups was subsequently merged to create a final design version.

Through the drive axle and an intermediate piezo balance the wing root is connected to a hydraulic actuator which allows the introduction of prescribed pitch excitations into the wing structure. The two control loops (see Figure 9) combine the input torque of the actuator with the output acceleration sensor signals from the wing root (inner loop) and wing tip (outer loop).

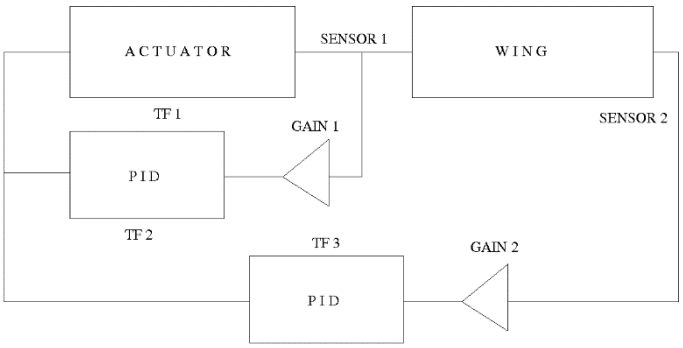

Figure 9: Structure and components of the ASE control loop with the two operation modes: ILC = only inner loop closed, OLC = inner + outer loop closed

They are designed to control the dynamic wind tunnel tests (ILC = only inner loop closed) and can be activated as a flutter suppression system (flutter break) in case of emergency (OLC = both inner and outer loop closed).

While the transfer function of the hydraulic actuator had been determined by component test measurements and a subsequent model matching, the transfer function behavior of the outer loop controller had to be found in an inverse approach by searching for a control characteristic that rendered the strongest additional damping effect on the flutter mode. By tuning the outer loop transfer function (see Figure 9) full authority over the aeroelastic wing system could be reached. In this sense the first flutter mode was eliminated from the range of the whole test parameters and thus the prior aeroelastic unstable system could be stabilized.

3.2.2 The structural Eigen modes

The mass and elasticity properties of the wing structure play a predominant role in the dynamic behavior of the aeroelastic system. In close reference to this fact, the range of the first five Eigen frequencies and the distribution of the clamped Eigen modes had been defined beforehand as main objective.

From the FEM described in Chapter 2 the Eigen modes and Eigen frequencies have been extracted and interpolated onto the aerodynamic panel mesh, see Figure 10. Through inspection of these surface plots, both the Eigen modes and the interpolation scheme have been checked. For the purpose of defining the right BC of the mounted wing, the elastic chain of suspension and drive elements (wing root, piezo balance, balance adapter and drive axle) have been composed diligently; further on to be called the “elastic BC”. The effect of the flexibility of the BC can be recognized in the considerable wing root pitch and even yaw deflection of the higher Eigen modes. Another apparent feature of some Eigen modes is the large angular deflection values of the engine nacelle relative to the spanwise wing station to which it is attached to. Thus in the fourth Eigen mode we can observe a strong nacelle pitching and in the sixth Eigen mode a predominant nacelle yawing coupled with a clear nacelle rolling motion.

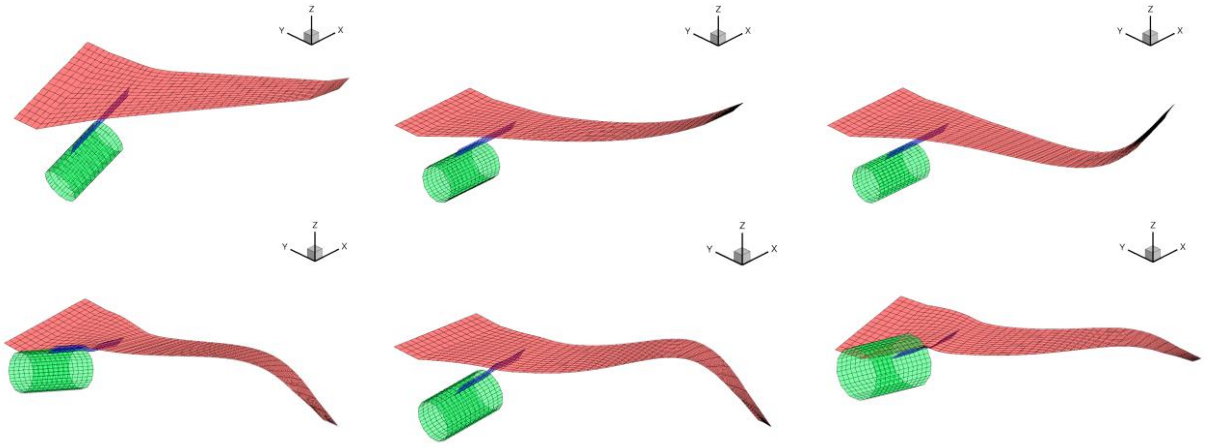

Figure 10: The first six structural Eigen modes (ILC) as interpolated on the aerodynamic panel mesh; rigid body pitch, 1st bending, 2nd bending, nacelle pitch/wing torsion, 3rd bending, nacelle yaw / wing lagging

3.2.3 Flutter analyses with the aeroelastic model

The results of the eigenvalue analyses were examined for a broad range of fluid densities and velocities. While the flutter modes of the critical first flutter cases always remain roughly the same with respect to appearance and modal composition, the eigenvalues differ strongly depending on the characteristics of flow. Being an important part of the modal results, the eigenvalues are presented in the shape of flutter curves as distributions of Eigen frequencies and aerodynamic excitation coefficients (for the matched Ma-number cases M=0.6, and M=0.7), see Figure 11. Please note that for the M=0.7 case, two different tip masses are included in the plot which were, among other parameters, part of the parameter study for the flutter analyses.

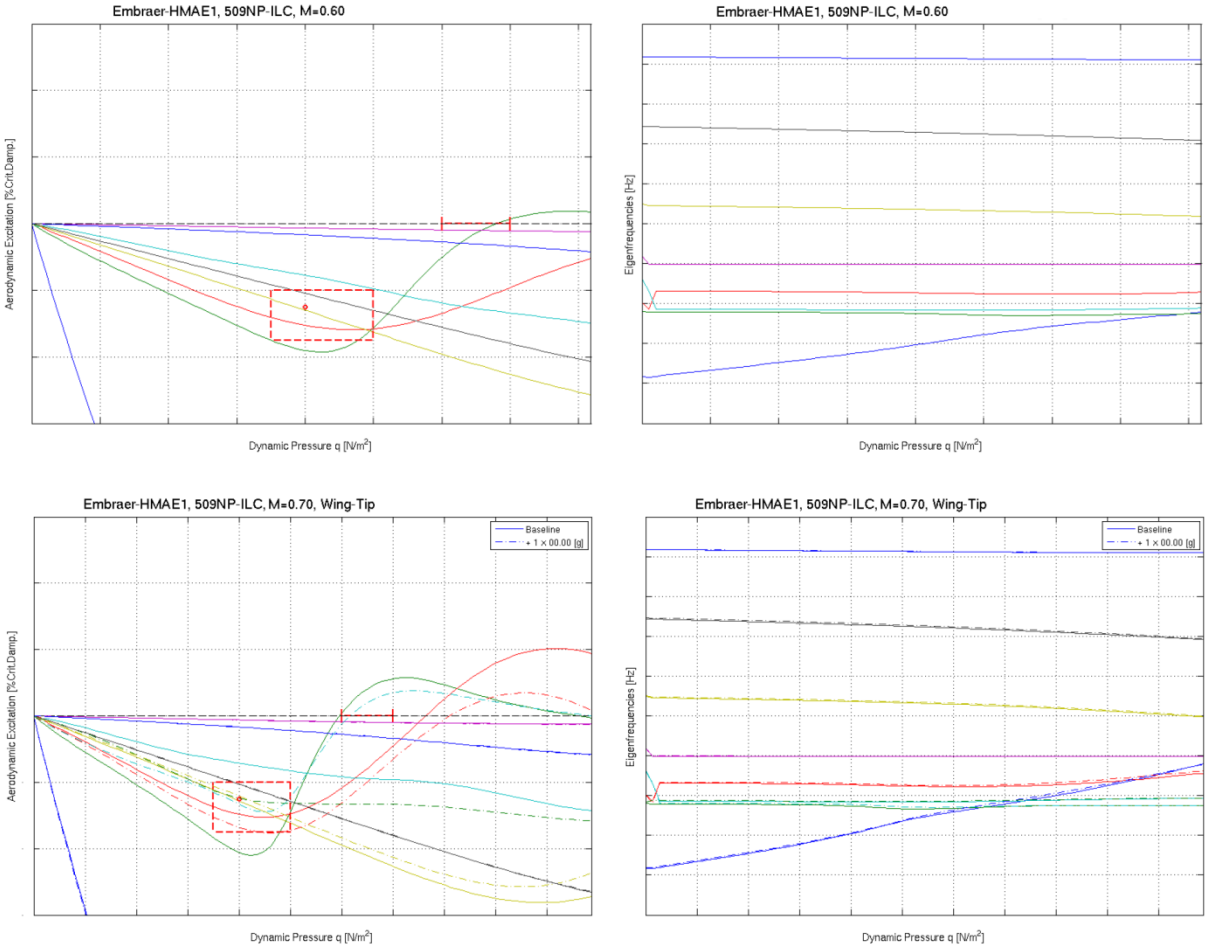

Figure 11: (upper) Flutter curves for M=0.60: normal operation (ILC) and (lower) M=0.7: normal operation (ILC) and two different wingtip mass cases. Red areas are the targets set by Embraer for maximum and zero damping.

Beside the Eigen frequencies and the critical air speed as the basic values of a flutter state, the respective flutter mode is the main feature of the dynamic instability. The highly complex Eigen mode gives a picture of the time-delayed wing deflection. In Figure 12 the flutter modes for the M=0.7 are presented in the shape of intermediate deflections between the extreme upper and lower position. The two corresponding flutter cases can be compared in the flutter diagram in Figure 11 as zero crossings of the damping curve, and also as participation factors in the flutter states in Figure 12.

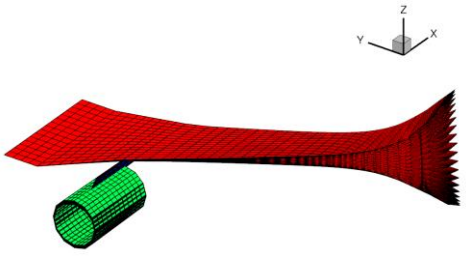


```
FLUTTER MODE 1 :
--------------------
MODE PARTICIPATION:
--------------------
1.)  0.3053    6.)  0.0441
2.)  1.0000    7.)  0.0719
3.)  0.5477    8.)  0.0505
4.)  0.2971    9.)  0.0022
5.)  0.0710   10.)  0.0202
--------------------
MODE PHASE (DEG):
--------------------
1.)  -20.27    6.)  146.97
2.)    0.00    7.)   -7.00
3.)  -43.45    8.)  176.51
4.)  147.64    9.)   -4.24
5.) -150.16   10.)  175.99
```

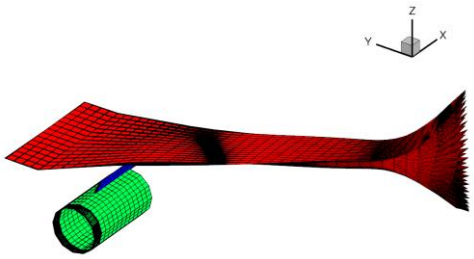

FLUTTER MODE 2 :

MODE PARTICIPATION:

1.)	0.2641	6.)	0.1492
2.)	1.0000	7.)	0.1233
3.)	0.4553	8.)	0.1025
4.)	0.5591	9.)	0.0046
5.)	0.9223	10.)	0.0376

MODE PHASE (DEG):

1.)	98.12	6.)	-55.50
2.)	0.00	7.)	3.09
3.)	2.21	8.)	179.02
4.)	129.70	9.)	12.04
5.)	135.62	10.)	177.99

Figure 12: The deflection cycle (M=0.7, ILC) of flutter mode 1 (up), and flutter mode 2 (down)

The first flutter mode appears as a combination of the first bending and torsion modes with a pure pitching content of the engine nacelle and a large deflection mainly in the outer span region of the wing. This indicates that also higher modes are involved, as it also can be seen in the table of the participation factors for the first 10 (of total 50) structural vacuum modes in Figure 12. With the first flapping mode being the 100% scaling reference mode, the second important contribution yields the second flapping mode with 55%. The basic torsional mode is the rigid body pitch of Eigen mode 1 with 30% participation, as it is the case of the elastic torsional motion of Eigen mode 4 with the counter pitching engine nacelle. The shown flutter mode can be considered representative for all the investigated test cases since its composition does not change strongly over the range of the test matrix. In contrast to flutter mode 1, the composition of flutter mode 2 shows additional high shares of the third flapping mode (92%) and the first lag/nacelle yaw/roll mode (15%), see in Figure 12. This is the outcome of a lateral bending of the drive train and results in an occurring nodal area in the mid-span region, to be seen in Figure 12. With varying updates done in the wing-to-pylon connection in the FEM, flutter mode 1 and 2 occurred to change order of position.

3.2.4 ASE flutter analyses with the aeroelastic model

The control components were assembled in two nested loops, with the closed inner loop being used for the control of a desired wing root pitch excitation, and the activated outer loop serving as a flutter break in case of emergency. The characteristics of the inner loop were given by the transfer function of the hydraulic actuator which beforehand had been identified from test measurement data (deflections, strains). In contrast to this, the characteristics of the outer loop controller had to be determined in an inverse sense by searching for the maximum damping increase. By activating the outer control loop for this purpose (simultaneously with the closed inner loop) the flutter crossings of the damping branch of the eigenvalues could be shifted upwards to higher dynamic pressure or completely suppressed, thus enabling full control authority over the flutter instability of the wing. Figure 13 shows the difference between the normal operation (ILC) and the flutter damper included for the calculations done with the version of the MSC Nastran FEM before the modal updating process.

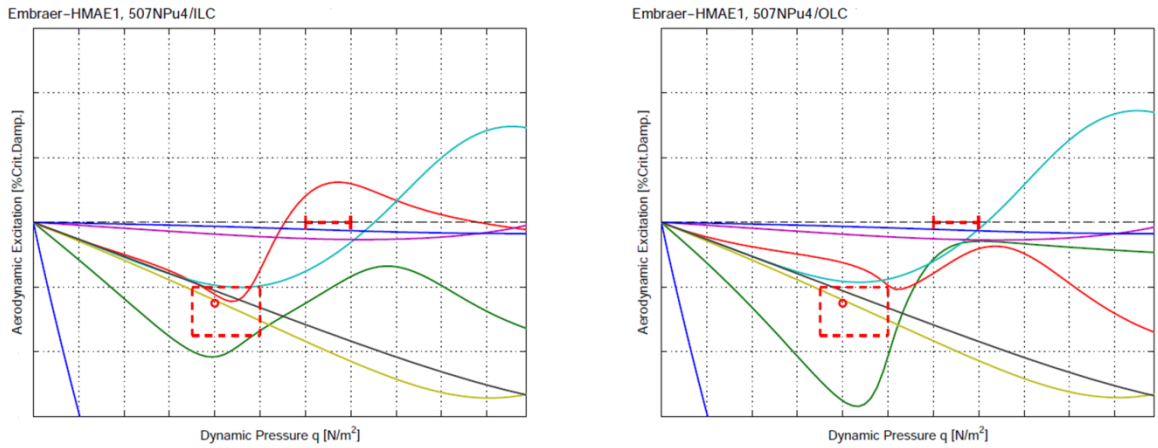

Figure 13: Damping curves for M=0.7 (CDR version), left: normal operation (ILC), right: flutter damper on (OLC)

The flutter calculations of the elastically suspended wing have been executed with the aeroservoelastic ASE module of the code ZAERO, where in contrast to a classical clamped beam (passive system) the BC need to have a non-restrained pitch condition in the controlled case. A comparison of the flutter points show that already the integration of the inner control loop with the experimentally identified transfer behavior of the hydraulic actuator has a positive impact on the wing stability by adding more damping to the system and thus shifting the flutter boundary upwards toward higher dynamic pressures. An additional activating of the outer control loop with its adjusted optimal transfer behavior will result in an even more damped and stable wing system with the flutter boundary moved to further upward values or even totally eliminated instabilities.

4 VALIDATION (BENCHMARK) TESTS

The maturity of the numerical FEM was determined through validation with experimental tests with a complete manufactured and instrumented wing. To generate input for the verification, bench tests, categorized in 4 items were started:

- Ground Vibration Test – initial,
- Static load / High Deflection test,
- Calibration of strain gauges,
- Ground Vibration Test – verification

The initial GVT provided measurement input of the fabricated model for FEM updates of wing, wing-to-pylon connection and wing-to-balance adapter (thus, without drive-train) to address the first five prescribed mode shapes and frequencies. The static load/high deflection test was meant to verify high deflection of the wing under the most critical loadcase. The loads were gradually built-up in order not to exceed the most severe loadcase as expected in the wind tunnel and possibly damage the model. Calibration of strain gauges was executed to provide a conversion matrix for sectional loads presentation. After finishing the static load test and calibrations, a second GVT session was performed, identical to the first one, to verify the integrity of the wing's dynamic response after being subjected to the effects of high loads and resulting large displacement.

The ground vibration tests were performed in a laboratory environment in the calibration facility of DNW-HST at both free-free (model suspended in springs) and clamped (model suspended to a heavy base support structure) boundary conditions to provide measured data to facilitate model-updating of the structural dynamic FEM.

A simplified wire mesh model was made of the single and combined components in order to directly check the outcome of the measurements of internal and external accelerometers with the mathematical model. As an example, a wire mesh is presented in Figure 14 for the WBPN configuration.

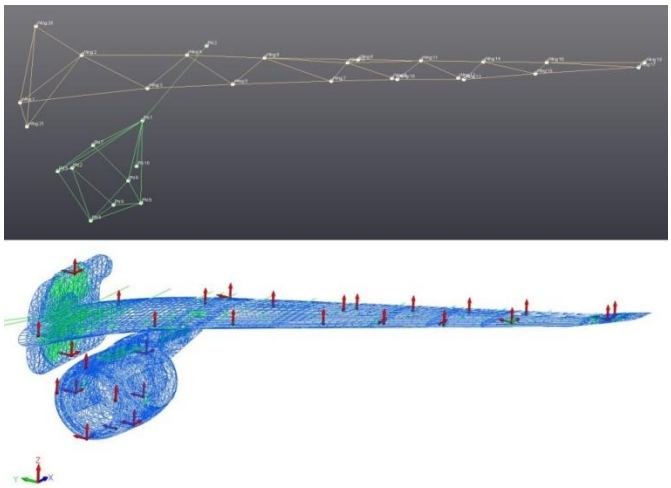

Figure 14: (upper) Wire mesh with node identification in LMS geometry and (lower) FEM representation of external and internal accelerometers used

The GVT started on the clamped pylon-nacelle only configuration at three different suspensions, all on a block on the concrete floor.

- Gravity acting on PN in lateral direction outboard (Figure 15, left);
- Gravity acting on PN in lateral direction inboard;
- Gravity acting on PN in vertical direction upwards (Figure 15, right).

A special adapter was designed and fabricated, simulating the lower wing contour. This was done to tune the PN in itself. With pylon-nacelle tuned individually and also the wing only tuned individually, differences between the FEM and tests results in the full configuration could be narrowed down to the wing-to-pylon connection (focus for the model updating process).

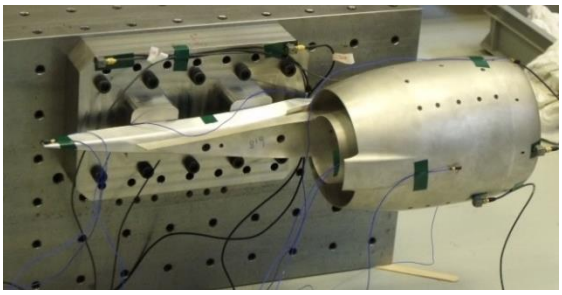

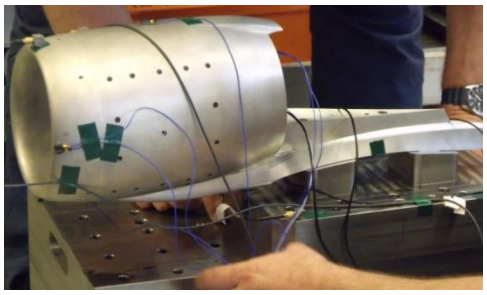

Figure 15: Pylon-nacelle only in different clamped conditions

The set-up of the GVT on the clean wing at clamped condition is presented in Figure 16, left. During the GVT excitation was introduced both by means of a shaker and hammer. An impression of the GVT set-up for the full wing-pylon configuration is presented in Figure 16, right.

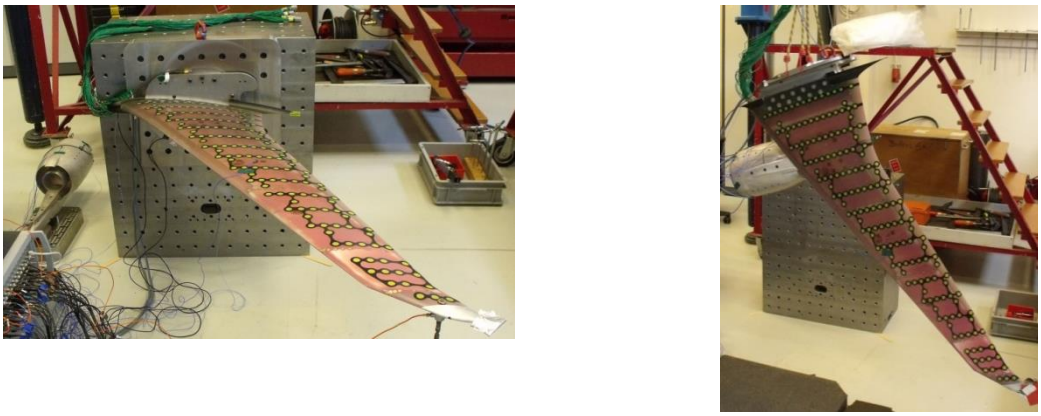

Figure 16: (left) Test set-up for the wing-only in clamped condition and (right) full wing-pylon in free-free condition

A representative Frequency Response Function (FRF) spectrum for full wing-pylon configuration in free-free condition with the majority of the frequencies visible is presented in Figure 17.

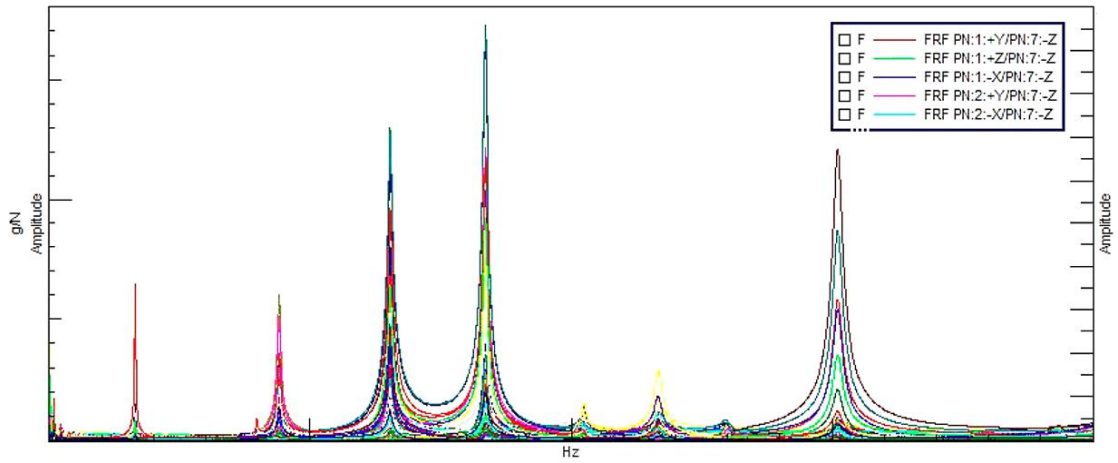

Figure 17: FRF for the full wing-pylon configuration in free-free condition

Once the initial GVT's were completed, the wing was equipped with the load application devices to execute the static load test for verification of high load bending, followed by calibrations of the strain gauges. The static tests were executed with the greatest care not to exceed the most severe loadcase as expected in the wind tunnel test program with following objectives:

- Demonstrate sufficient strength for the maximum deflection loadcase.
- Demonstrate the required deflection level for the maximum deflection loadcase.
- Demonstrate that wing section loads at four wing stations specified can be predicted with sufficient accuracy using the installed set of strain gauge bridges.
- Verification and validation of the FEM stiffness by means of a limited number of vertical displacement measurements along the span.
- Characterization of non-linear effects.

These objectives lead to the following static test set-up:

- A set of seven discrete point loads were defined that are equivalent to the maximum deflection loadcase. Internal loads for the equivalent loadcase never exceed the highest local internal loads (limit loads) as expected during wind tunnel testing.

Note that the structure is designed for a safety factor 3.5 for this load condition as required by DNW. All point loads are generated by gravity loads on external masses. As the aerodynamic load on the wing is in upward direction, the WT model is installed upside down in the test rig, see Figure 18, left.

- The discrete point loads represent the resultant aerodynamic loads on portions of the windtunnel model between two wing stations. The single F_z is selected in such a way to generate the same F_z, M_x and M_y resultants as the original aerodynamic load.
- A set of Load Application Devices (LAD) was designed to apply these discrete loads to the HMAE1 model. These consist of a total of six clamps on the wing and a fitting for introducing loads in the upper pylon (Figure 18, left). The clamps are designed to tightly fit around the local model contour. A thin rubber layer prevents local point loads to be introduced in the skin of the wing. FE analyses on the clamping devices show that wing torsion moments are mainly balanced by vertical loads at the leading and trailing edge. Friction loads that prevent sliding of the clamps are limited. Hence, the wing is inclined at its root by 25 degrees, upside down. The 25 degrees equal the expected maximum deflection angle at the wing tip. As a result, the clamps will always have a tendency to slide towards the root. The increase of profile thickness in that direction will prevent sliding of the clamps.
- All loading conditions are applied in steps from 0% to 100% and back to 0% load level in order to capture non-linear responses and any hysteresis.
- Vertical displacements are measured at all load rods connected to the load introduction devices during limit load testing. This allows computation of relative movements of points on the wing, thus measuring wing flexibility independently of the support flexibility. Furthermore, the absolute tip displacement was measured relative to the laboratory floor with a laser distance measurement device. The root inclination (roll angle) was measured with an electronic leveling device. This allowed correcting relative displacements of points on the wing with respect to the wing root.

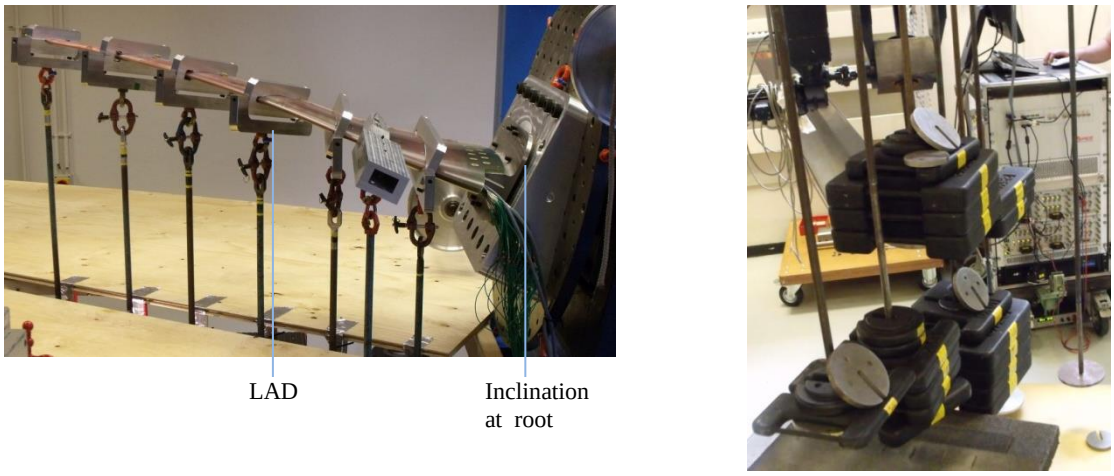

Figure 18: Wing in upside position including the load application devices (left) and steel or cast iron blocks to act as loading masses

The Skopinski method [5] is used to predict section loads (shear, bending and torsion) from strain gauge readings. This requires the application of a sufficiently varied set of load conditions. These calibration loads are applied by means of the load introduction devices.
In order to increase variation in wing torsion, apart from the nominal load point position, additional loading points are added to each wing LAD and the pylon LAD.

After finishing the static load test and calibrations, a second GVT session was performed, identical to the first one, to verify the integrity of the wing dynamic response (frequencies and mode shapes), after being subjected to the effects of high loads/large displacement. From this GVT it was concluded that no damage was inflicted to the wind tunnel model.

5 MODEL VALIDATION

After completion of the critical design review, manufacturing of the model started by the NLR. During and after the manufacturing process, the MSC Nastran numerical model was updated and validated to obtain a high correlation with the manufactured model. This is done based on ground vibration tests.
After the tests completed, a final step was to compare the numerical model with test measurement results. This paper shows the correlation in static deformation between the SPR measurements and static aeroelastic analyses.

5.1 Ground vibration tests

After the HMAE1 wind tunnel model was manufactured several GVT's have been executed to understand the structural dynamic characteristic. The physical MSC Nastran model is updated based on the results from these GVT's. Major updates have been done on the connection between components since the modelling of this interface showed to have a signifcant influence on the correlation with the tests. The final updated model shows high Modal Assurance Criterion (MAC) values and matched frequencies for the first five Eigen modes.

Due to various GVT's at component level, model updating was first focused on the different components, i.e. wing only and pylon-nacelle only, after which the full configuration update focused on the wing-to-pylon connection. Figure 19 shows the modeshape comparison between the test model (red wireframe) and FEM (blue) for the first two wing-only modes in the free-free boundary conditions.

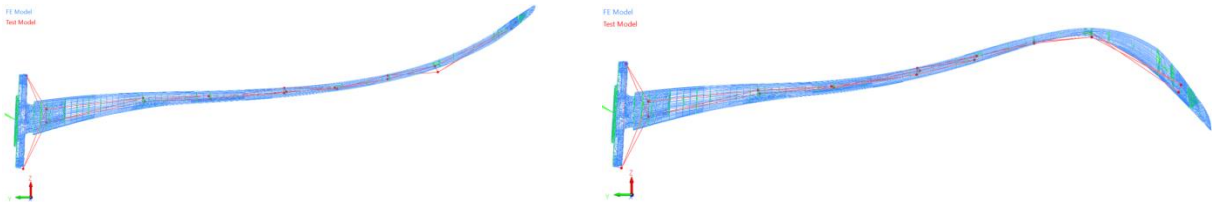

Figure 19: (left) Wing only modeshape pair for the first bending and (right) second bending mode

Updates to the wing model included small changes to the center of gravity as well as updates to the laminate properties. The updates only included minor changes to the model such that the properties were still a physical representation of the materials used during manufacturing.

For the pylon-nacelle, updates have mainly focused on mass properties since there was no uncertainty in the stiffness properties of the material. Figure 20 shows the correlation of the test results (red wireframe) with the FEM (blue) of the pylon-nacelle in free-free condition for the first two modes.

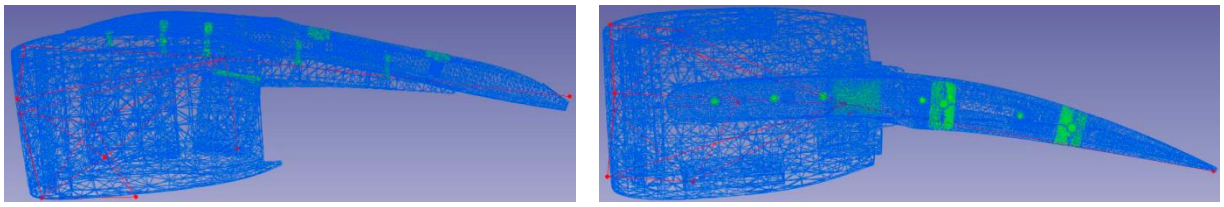

Figure 20: Pylon-nacelle modeshape pair, (left) side view showing the vertical-bending mode, (right) top view showing the side-bending mode.

After updating the wing and pylon-nacelle separately, the combined model can be updated, focusing on the connection between the wing and pylon nacelle. Updates to the wing-to-pylon connection were mainly focused on the load path that resulted from the manufacturing process. Within the initial FEM the load was transferred from the pylon to the inner metal inserts attached to the lower wing skin. During assembly, adhesive was used to attach the lower to the upper part which resulted in an additional load path from the metal insert to the foam and upper skin, see Figure 21.

Figure 21: Metal inserts for the pylon to wing connection which have also have been covered in adhesive (not shown in the image) during full assembly, resulting in an additional load path

The update in wing-to-pylon connection was included in the FEM and in the end a high correlation in MAC and frequency was found for the first 10 modes compared to the test results. See Figure 22 for the correlation of the pylon pitch mode with the GVT results performed outside of the windtunnel (fixed boundary conditions on a support structure).

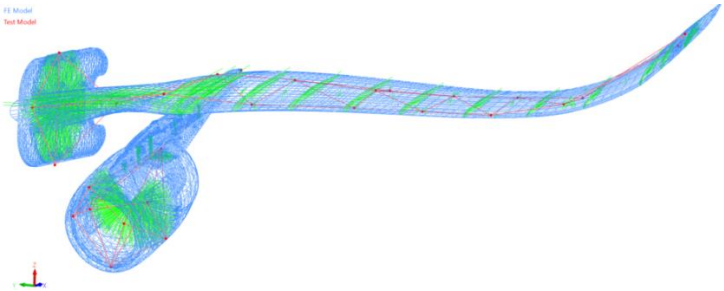

Figure 22: Pylon pitch mode correlation between the FEM (blue) and test wireframe (red)

In a final step, a GVT was performed by DLR inside the windtunnel (see Figure 23, left) in order to update the high fidelity drivetrain (the actual boundary condition used during the tests). One of the significant updates for the drivetrain was the constraints initially used for the bearing (number 3 and 4 in Figure 23, right). The tapered roller bearing and thereby the axle was initially constraint in the x and z direction. However, based on GVT results this degree of freedom was included.

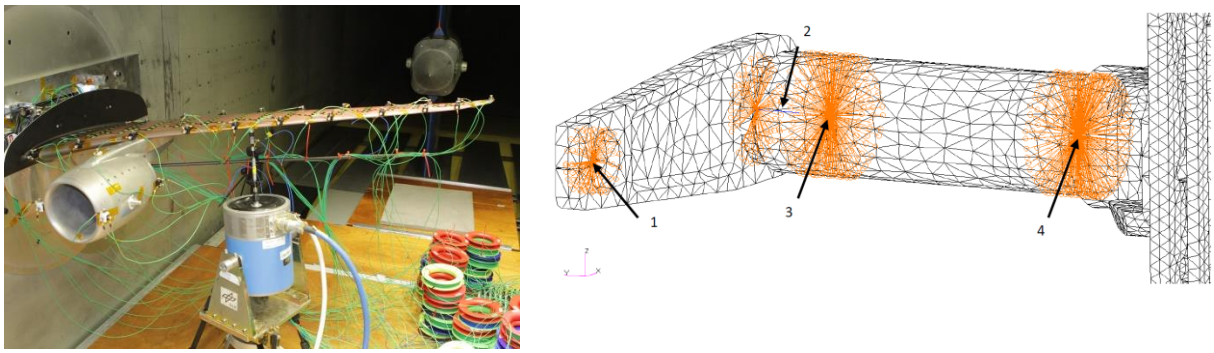

Figure 23: GVT set-up inside the windtunnel performed by DLR and (right) drivetrain constraints for the lever and axle in the FEM

The final updated FEM including the high fidelity boundary condition showed a high correlation for different configurations tested with the manufacturing model. Figure 25 shows the high MAC correlation between the full FEM and final GVT results inside the windtunnel set-up and Figure 25 the first mode correlation.

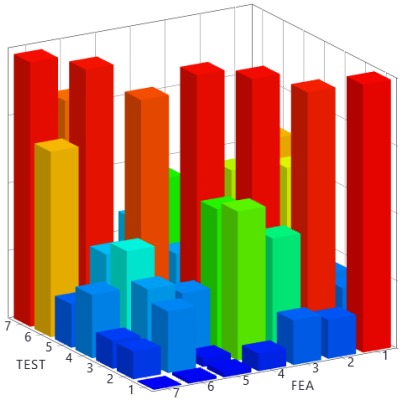

Figure 24: MAC values between the FEM and windtunnel GVT results performed inside the test section

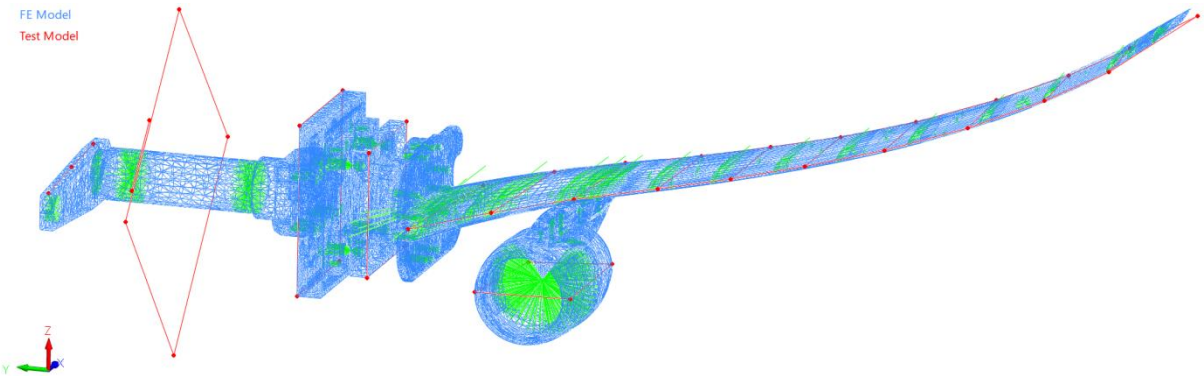

Figure 25: Correlation between the test results (red) and the full FEM including drivetrain (blue) for the first wing bending mode

5.2 Windtunnel test correlation

During the test, the displacements of the model have been measured using SPR. On the upper side of the HMAE1 model, markers have been placed in chord and spanwise direction, see Figure 1. The deformation of the model is obtained by following the markers during the tests. The position of the markers is measured at various steps; at AoA = 0 [deg] (wind off), at the nominal AoA (wind off) and in wind on situation.

The delta displacement is obtained by the difference between the nominal wind off angle of attack measurement and the final wind on measurement.

One of the main goals set by Embraer was to study the effect on the aeroelastic characteristic associated to the high flexibility of high aspect ratio wings. To achieve this goal it was a requirement to develop a model that reached a wing tip displacement in the order to 12%-16% semi-span for the maximum loading condition. From the SPR measurements, it can be concluded that the loadcase resulting in a maximum wing tip displacement was indeed the critical loadcase assumed during the design study. Also from piezo balance data, the maximum normal load is obtained for this test condition. This test condition resulted in a maximum wing tip displacement equal to 17.5% of the semi span at the location of the last SPR marker (no SPR markers placed on the wing tip).

During the correlation analysis for the static deflection use is made of a linear aeroelastic solver based on Vortex Lattice Method (VLM) aerodynamics and integrated pressure data from pressure measurements done during the tests. Figure 26 shows the correlation between the aeroelastic analyses using the updated FEM (red, FEM top skin nodes) and the SPR measurements (black) for the critical load case.

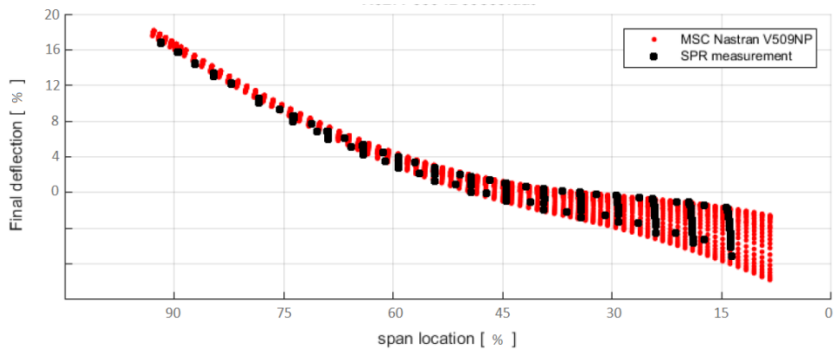

Figure 26: Comparison between the aeroelastic analyses using the final updated FEM and SPR measurements for the critical load case

For the case of the highest dynamic pressure, VLM aerodynamics showed an overestimation of the static displacements compared to the SPR measurement. A better agreement was found using the integrated pressure in combination with a geometric non-linear solver, shown in Figure 27.

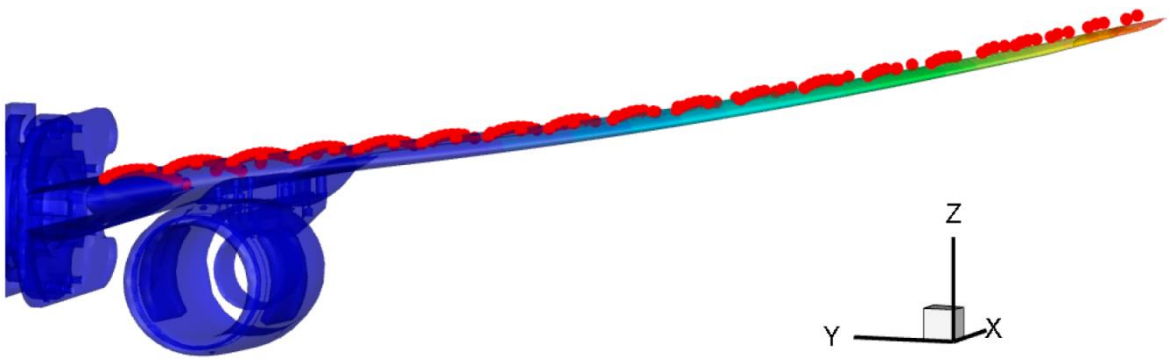

Figure 27: Correlation between the FEM and SPR measurements for a high dynamic pressure case and M = 0.6 using integrated pressure data

Because no pressure data was available on the nacelle, wing only test cases have also been compared to the FEM, excluding the pylon-nacelle, in combination with the geometric non-linear solver. Figure 28 shows the wing only configuration tested at M = 0.7, Q = 4.44×10^4 [Pa] and AoA = 0 [deg]. A good correlation can be observed between the FEM displacements and SPR measurements.

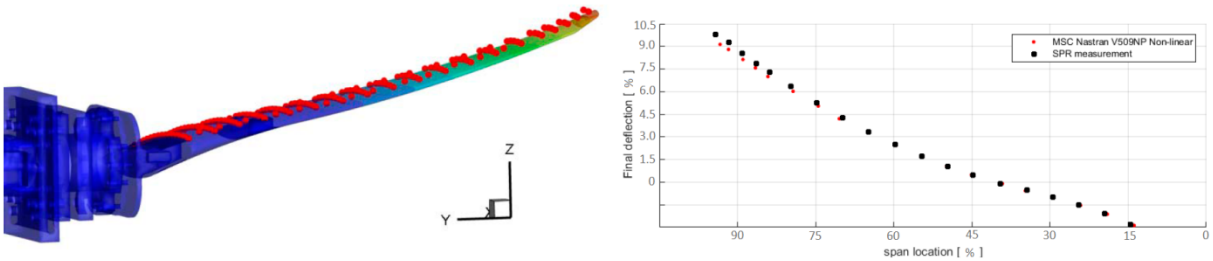

Figure 28: Correlation between the FEM and SPR measurements for a wing-only case using integrated pressure data

6 CONCLUSIONS

The HMAE1 project was initiated to study the effect on aeroelastic characteristics associated to the high flexibility of high aspect ratio wing. To achieve this goal, a highly elastic fiberglass wing-body pylon nacelle wind tunnel model is developed, manufactured and tested in the DNW-HST transonic wind tunnel. The main objectives to study these effects set by Embraer were:

- An aeroelastic wing model with high deflection,
- A target for the first five prescribed modeshapes and frequencies,
- A target for the required flutter mechanism,
- A target for the dynamic aeroelastic model behavior in terms of damping

During the design phases, a numerical structural dynamic Finite Element Model is developed and, in the end, updated and validated using ground tests. A static load test and several ground vibration tests outside and inside the windtunnel have been executed to determine the structural dynamic behavior of the single components and the interaction between these components. The numerical Finite Element Model shows high modal assurance criterion and matched frequencies for the first five Eigen modes for various test configurations.
After extensive flutter analyses, varying many parameters (both aerodynamic conditions as well as various mass configurations and control loops), the final aeroelastic model including the updated Finite Element Model has shown that the required mechanism occurs due to the interaction between the first two modes. In addition, the maximum damping and zero damping (flutter point) of this flutter mode matched the targets set by Embraer.

The HMAE1 manufactured model has shown the required high deflection and has shown the beginning of deterioration of damping for the flutter mechanism inside the Test Matrix. This allows the extrapolation of the points to determine the flutter speed outside the test matrix region.

Overall, it can be concluded that the aeroelastic requirements set by Embraer have been fulfilled and that this model allows investigating static and dynamic aeroelastic characteristics of aircraft wings presenting large displacements.

7 REFERENCES

[1] Govers, Y., et al, “Wind Tunnel Flutter Testing on a Highly Flexible Wing for Aeroelastic Validation in the Transonic Regime within the HMAE1 Project”, IFASD 2019, Savannah, Georgia, USA

[2] NLR news, https://www.nlr.org/news/aircraft-of-the-future-researchers-conduct-first-real-time-flutter-analysis/, 2018

[3] Jelicic, G., Schwochow, J., Govers, Y., Sinske, J., Buchbach, R.,Springer, J. (2017). “Online Monitoring of Aircraft Modal Parameters during Flight Test based on permanent Output-Only Modal Analysis”, in 58th AIAA/ASCE/AHS/ASC Structures, Structural Dynamics, and Materials Conference, American Institute of Aeronautics and Astronautics.

[4] Boeswald, M., et al, "Online monitoring of flutter stability during wind tunnel testing of an elastic wing with pylon and engine nacelle within the HMAE1 project", IFASD 2019, Savannah, Georgia, USA

[5] Skopinski, T.H. e.a, ”Calibration of strain-gauge installations in aircraft structures for the measurement of flight loads”, NACA report 1178

In memoriam of Bimo Prananta, who was heavily involved in the startup of the HMAE1 project.

COPYRIGHT STATEMENT